PROCEEDINGS OF SCIENCE

Microwave imaging spectroscopy of the Solar corona

S. V. Lesovoi,[a,*] **M. V. Globa,**[a] **A. V. Gubin**[a] **and A. T. Altyntsev**[a]

[a] *Institute of Solar Terrestrial Physics, Lermontov Str. 126a, Irkutsk, Russia*

E-mail: svlesovoi@gmail.com

The study of the solar corona plays a key role in understanding solar activity. Microwave imaging spectroscopy - measuring microwave spectra at every point on the solar disk (or image) - is the most promising method for studying the lower corona and the chromosphere-corona transition region. Solar microwave emission originates in the low corona and in the upper chromosphere and is produced both by thermal and non-thermal electrons. The main types of emission are bremsstrahlung, gyroresonance and gyrosynchrotron emission. The quiet Sun emission is dominated by the bremsstrahlung while the active region emission is due to the gyroresonance mechanism. The gyrosynchrotron emission is generated by non-thermal electrons during solar flares. Microwave emission spectra allow us to estimate the temperature and density of the plasma in active regions. Microwave spectroscopy of the solar corona is perhaps the only method for measuring the coronal magnetic field both for the quiet Sun and for transient events.

The Siberian Radioheliograph (SRH), a new generation solar radio telescope, is described, and the first observations of solar activity in the broadband frequency range 3-24 GHz are presented. The estimation of the magnetic field scale length is presented. The scale length was estimated by using the SRH data – spectra of an active region emission in the frequency range 3–12 GHz.

The Multifaceted Universe: Theory and Observations - 2022 (MUTO2022)
23-27 May 2022
SAO RAS, Nizhny Arkhyz, Russia

*Speaker

PoS(MUTO2022)014

1. Introduction

Although the promise of microwave imaging spectroscopy (MIS) for solar physics has long been recognized ([1], [2], [3]), there are still no completed projects that meet all the requirements of MIS. Perhaps the most successful radio telescope designed for MIS is the Expanded Ovens Valley Solar Array (EOVSA). The project includes both a broadband solar radio telescope and software (GX Simulator [4]) to simulate corona plasma parameters (density, temperature, magnetic field) that are consistent with microwave data augmented with EUV and X-ray data. Promising results have been obtained in coronal magnetography [5], although the small number of antennas makes full disk imaging difficult. The Mingantu Spectral Radio Heliograph (MUSER), another broadband solar telescope, is still under construction. The Siberian Radioheliograph (SRH) is also a MIS dedicated radio telescope. RATAN-600 successfully observes the Sun, albeit in 1-dimensional mode, but in a very broadband frequency range [6]. SRH is currently in final testing mode. The start of routine observations is scheduled for 2023. SRH should fully cover the lack of spectrally and spatially resolved solar microwave observations in the 0 - 10 UT range. There are interesting studies of the outer solar corona at metric wavelengths made by the Low Frequency Antenna Array (LOFAR) and Murchison Widefield Array (MWA) ([7], [8], [9]), although LOFAR and MWA are not solar dedicated instruments.

The imaging spectroscopy of the solar corona aims to study both flaring and non-flaring activity. The main tasks are to measure the magnetic field, determine the traces of electron beams, and estimate the flare productivity of the active region. Of particular interest is the study of coronal mass ejections (CMEs). MIS is a powerful method to model CME events more adequately [10]. Below, we describe the SRH and give several examples of SRH spectral data.

2. SRH description

SRH consists of three T-shaped antenna arrays (Fig. 1) operating in the frequency ranges 3–6, 6-12, 12–24 GHz ([11]). Arrays 3-6 are oriented in the east-west-north direction, and arrays 6-12 and 12-24 are oriented in the east-west-south direction. The fundamental spacing (9.80, 4.90 and 2.45 m) is chosen to meet the Nyquist criterion for sampling of the spatial spectrum of the Sun at the lower frequencies of each band. The angular size of the Sun corresponds to the spatial frequency $u_{sun} \approx 100$, and the fundamental SRH spacing at the lower frequency of each array is always less than 98. The 3–6 and 6–12 arrays are uniform, and the 12-24 array has increasing spacing with a uniform central part (similar to Nobeyama Radioheliograph [12]). The antenna diameters are 3, 2 and 1 m, respectively. The accumulation time can vary in the range of 0.01–0.10 s. SRH signal and data processing corresponds to the 48-antenna SRH prototype described in [13, 14]. Namely, the RF signal from the dual circular polarization feeds is transmitted to the working room by RF-over-fiber links, one polarization at a time. After down-conversion to IF ranging from 10 to 50 MHz, the signal is input to a 12–bit 100 Msps ADC. This is followed by delay tracking and fringe stopping, performed by delay lines, fractional delay filters and second local oscillators phase control. The delay tracking and fringe stopping accuracies are 0.1 s and 0.3 degrees, respectively. Complex IQ data (analytical signals) are input to a complex correlator operating in 1-bit or 4-bit mode. The correlator output – complex visibilities – are available on the local network. The daily

Figure 1: The central part of SRH antenna arrays. The back row is the 3-6 GHz array, which has 3-meter dishes and 9.8 meters spacing between the antennas, middle row is the 6-12 GHz array with 2-meter dishes and spacing of 4.9 meters, and the smallest antennas are the 12-24 array with 1-meter dishes, whose center has 2.45 meters spacing.

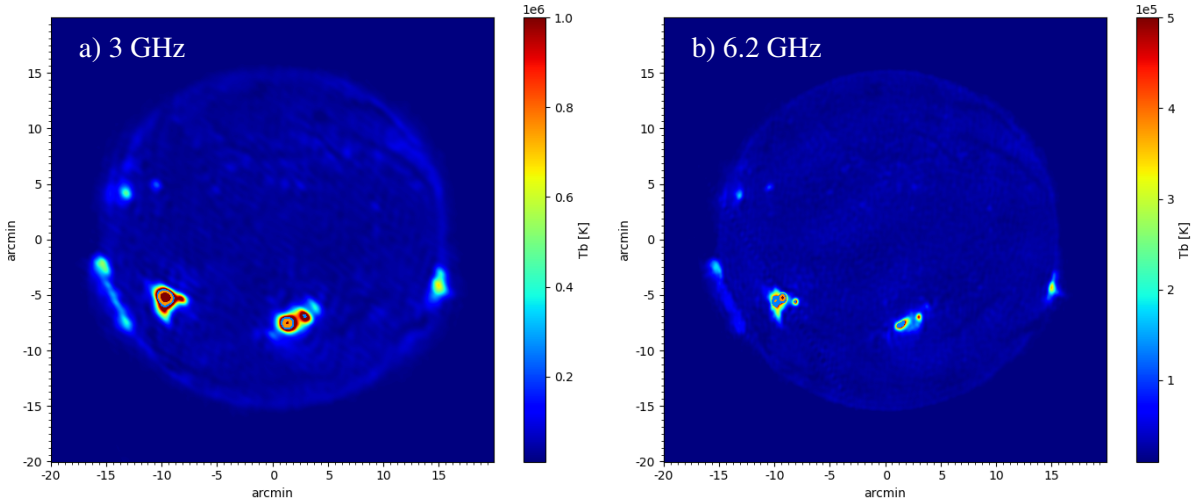

Figure 2: May 11, 2022 at 03:00 UT. Microwave images of the Sun, obtained by SRH at a) 3.0 GHz and b) 6.2 GHz. Brightness temperatures greater than 0.5×10^6 K for a) and greater than 1.0×10^6 K for b) are shown by filled contours. All features of the solar activity (active regions, prominences) are distinctly seen against the background of the solar disk.

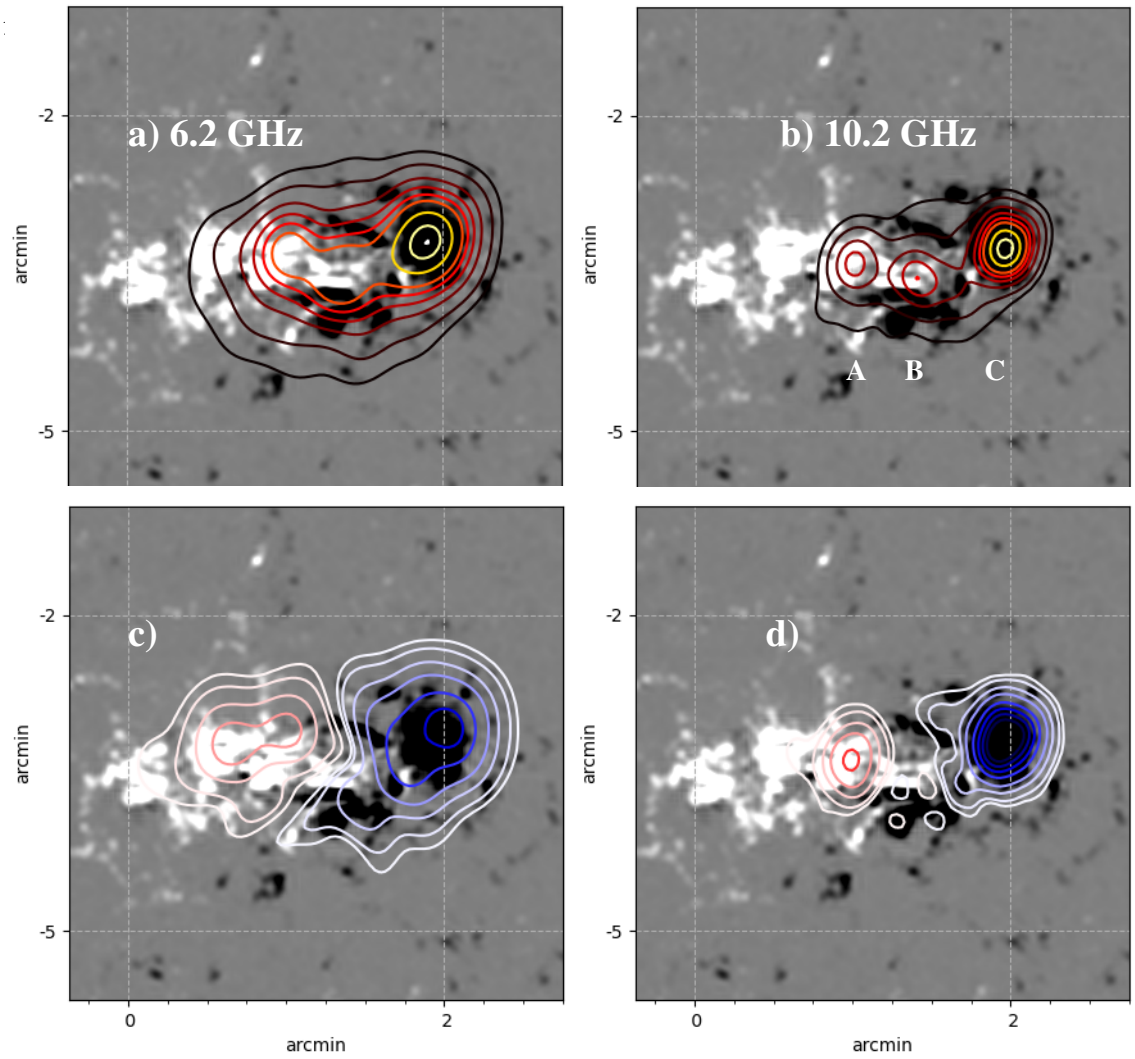

Figure 3: SRH intensity (I) (panels a, b) and polarization (V) (panels c, d) contours at 6.2 GHz, 10.2 GHz are plotted over an HMI magnetogram of AR13004. Data were obtained on May 4 2022 at 03:40 UT. Spectra of sources denoted by A, B, C in panel b) are shown below. The position of the source B is near the magnetic neutral line. This AR was chosen to demonstrate the microwave imaging spectroscopy with SRH because it is close to the central meridian.

volume of SRH data in routine mode is about 115 GB. The SRH spatial resolution reaches 5 arc seconds and the temporal resolution reaches 20 ms.

Table 1 shows some parameters of SRH arrays that affect the image quality. Gain calibration is proposed to be carried out using the redundancy of SRH antenna arrays. The ratio of the full number of baselines (N_{full}) to the number of redundant ones (N_{red}) is about 2 for all arrays. In other words, we use about half of the measured visibilities for imaging and the remaining half is used for calibration. Gain calibration is in fact solving a system of nonlinear equations containing complex antenna gains, assuming that the same (redundant) baselines should give the same visibility. The phase noise of the snapshots after calibration using the redundancy is about 10^3 for arrays 3–6 and 6-12, and $< 10^2$ for array 12–24. Further improvement of the images is possible by using self-calibration with a starting model, obtained from redundancy calibration, and the 12-24 array

Table 1: The SRH antenna arrays parameters. N_A – full antenna number in array, Orient. – array orientation, D – dish diameter, FOV – field of view, b_0 – shortest baseline (fundamental spacing), N_{full} – full number of visibilities, N_{red} – number of redundant visibilities, u_{max} – highest spatial frequency, θ_{min} – highest spatial resolution

N_A	Orient.	D [meter]	FOV [degree]	b_0 [meter]	N_{full}	N_{red}	u_{max}	θ_{min} [arcsec]
129	N32-EW97	3	0.9–1.8	9.80	8256	5152	18816	15
192	S64-EW128	2	0.9–1.8	4.90	18336	10144	24892	12
207	S68-EW139	1	0.8–1.5	2.45	21321	11869	61544	5

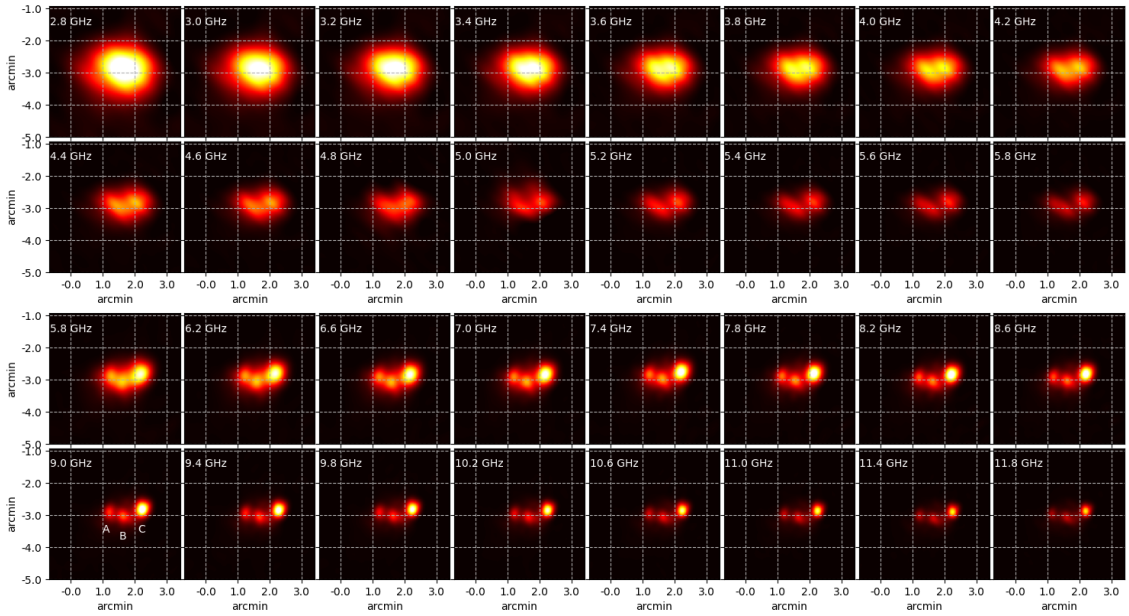

Figure 4: The images of AR13004 in the 2.8–11.8 GHz frequency range. The upper two rows are data from the 3-6 GHz array, the lower ones – 6-12 GHz array. The maxima of the brightness temperature scales are $6 \times 10^6 K$ and $2 \times 10^6 K$ for 3-6 and 6-12 data.

also requires a slight modification to the front end of the antenna. The total dynamic range of SRH receivers of more than 30 dB is sufficient for observing flare driven microwave bursts. The relatively large field of view of SRH and high sensitivity make it possible to observe CMEs from the solar disk at a distance of up to the solar radius. Figure 2 shows images of the Sun at the frequencies 3.0 GHz (a) and 6.2 GHz (b) obtained by SRH on May 11, 2022 at 03:00 UT.

3. Observations

Let us consider an example of the gyroresonance sources belonging to AR13004 observed with SRH on May 4, 2022. Figure 3 shows superimposed SRH images at frequencies 6.2 GHz, 10.2 GHz, and the SDO/HMI magnetogram. We are interested in what can be said about the strength and scale length of the magnetic field and about the nature of the unpolarized source, denoted by the letter B in panel b) of Figure 3. Figure 4 shows the data set in the 3-12 GHz frequency range obtained by

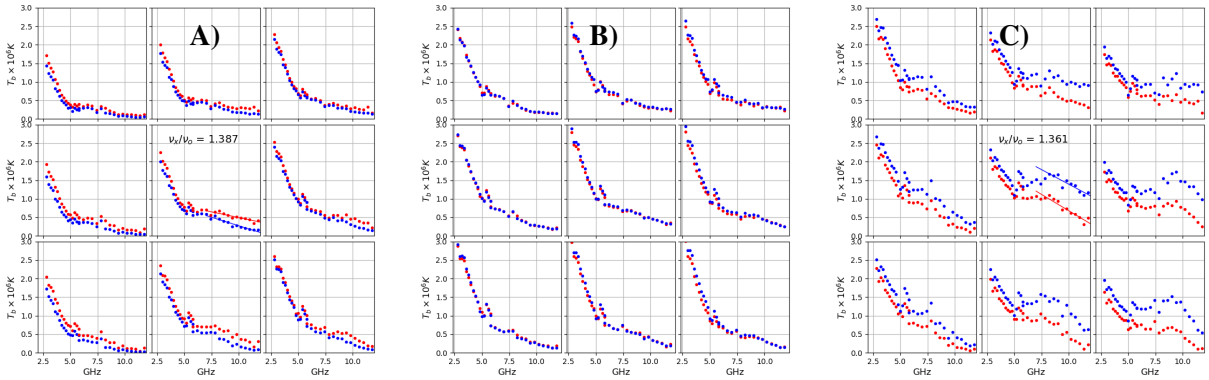

Figure 5: Brightness temperature spectra measured at 9 points near the peak of each source A, B, C indicated in Figure (3, 4). The red and blue lines show RCP and LCP, respectively. Sources A and C are gyroresonance sources, source C is located in a stronger magnetic field with respect to source A. Source B is probably the so-called neutral line associated source. The features (outliers) on the plots near 6 GHz are due to the non-ideal absolute brightness temperature calibration.

3-6 and 6-12 antenna arrays. Different saturation levels for 3-6 and 6-12 are chosen so that weak sources at higher frequencies are distinctly seen.

The brightness temperature spectra at the points in the vicinity of the maximum of sources A, B, C are shown in Figure 5. Free-free emission dominates at low frequencies, gyroresonant emission contributes in the range of 5-12 GHz. The central plot of each panel of Figure 5 is the spectrum of the brightest point of the sources. Such spectra are least affected of all by the SRH beam. The spectra of the vicinities of the brightest points decrease towards higher frequencies due to the decrease in the size of the response with frequency. This is one of the important reasons for using physical emission region models, i.e. the GX simulator, when processing microwave data. The absolute value of the magnetic field strength in the transition region can be estimated from the linear regression of the high-frequency parts of the spectra ([15]). The results of the linear regression are shown in the central plots of panels A) and C). The ratio of x-mode and o-mode cutoff frequencies is 4/3 rather than the expected 3/2. Therefore, we will calculate the magnetic field under the assumption that the 4th harmonic of the gyro frequency dominates in the x-mode. This results in about 1600 and 1550 gauss for the x-mode and o-mode of source A. These values for source C are about 1690 and 1650 gauss. The SDO/HMI photospheric magnetogram gives 1750 and 2130 gauss. Source B is most likely not related to coronal currents, its emission is dominated by a free-free mechanism and loop top emission with a viewing angle close to 90°.

The gyroresonance opacity depends on the scale length of the magnetic field $B/\frac{\partial B}{\partial l}$ ([16]). If it is possible to measure the scale length, then information about the 3D structure of the magnetic field can be obtained. As is evident from the images in Figure 5, the distance between sources A and C increases with increasing frequency. This can be explained by the different locations of the gyroresonance layers (GRL) along a magnetic loop. In the assumption that the loop is an arc of a circle, the height of GRLs depends on frequency. Fitting the height dependence of GRL to an exponential curve $B(h) = B_0 \exp(-h/\Delta L)$ results in $\Delta L \approx 11.6 \times 10^3$ km (Figure 6 b)). As one can see in Figure 5 A) and C) the difference $T_x - T_o$ for source C is about twice that for source A at

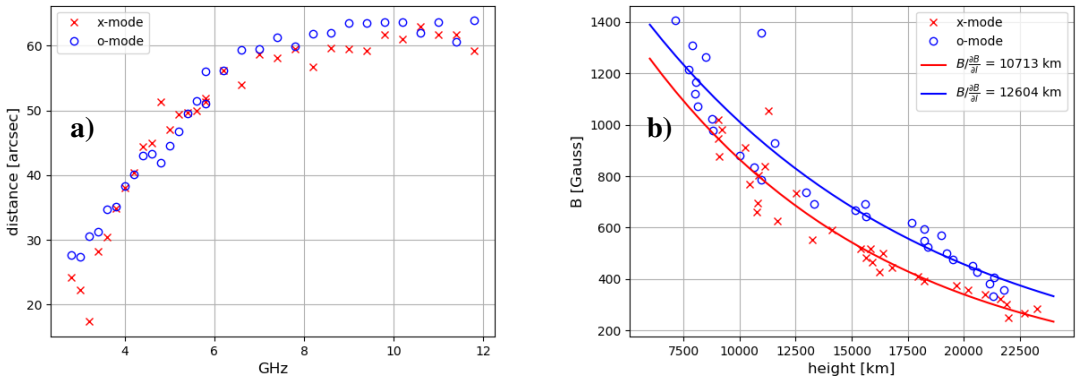

Figure 6: Panel a) shows the dependence of the distance between sources A and C on frequency. The distances for the x-mode and o-mode are the same at lower frequencies where the free-free emission dominates and are different at higher frequencies where most contribution is due to the gyroresonance emission. The o-mode distances exceed the x-mode ones because the o-mode GRLs are below the x-mode GRLs. Panel b) shows the dependence of the magnetic field strength on height above the loop feet location. The excess of strength obtained from the o-mode data is due to the fact that the contribution of free-free emission increases at heights above 15×10^3 km.

frequencies higher than 6 GHz where gyroresonance dominates. It follows that the loop is not an arc of a circle and $\Delta L_A \approx 2\Delta L_C$. Since we were estimating the mean value of ΔL, we can assume $\Delta L_A \approx 7.6 \times 10^3$, $\Delta L_C \approx 15.1 \times 10^3$ km.

4. Conclusion

We have considered how the SRH meets the requirements of microwave coronal spectroscopy. We have shown that from SRH observations of gyroresonant sources it is possible to estimate the scale length of the coronal magnetic field.

Acknowledgements

The work was financially supported by RSF (Grant No. 22-22-00019).

References

[1] J. Lim, D.E. Gary, H.G. J. and J.R. Lemen, *Imaging Spectroscopy of Solar Microwave Radiation. I. Flaring Emission*, *Astrophys. J.* **430** (1994) 425.

[2] D.E. Gary, G.D. Fleishman and G.M. Nita, *Magnetography of Solar Flaring Loops with Microwave Imaging Spectropolarimetry*, *Sol. Phys.* **288** (2013) 549.

[3] G.D. Fleishman, G.M. Nita, B. Chen, S. Yu and D.E. Gary, *Solar flare accelerates nearly all electrons in a large coronal volume*, *Nature* **606** (2022) 674.

[4] G.M. Nita, G.D. Fleishman, A.A. Kuznetsov and D.E. Gary, *Three-dimensional Radio and X-Ray Modeling and Data Analysis Software: Revealing Flare Complexity*, *Astrophys. J.* **799** (2015) .

[5] D.E. Gary, B. Chen, B.R. Dennis, G.D. Fleishman, G.J. Hurford, S. Krucker et al., *Microwave and Hard X-Ray Observations of the 2017 September 10 Solar Limb Flare* , *Astrophys. J.* **863** (2018) 83.

[6] V.M. Bogod, T.I. Kaltman, N.G. Peterova and L.V. Yasnov, *Study of the magnetospheres of active regions on the sun by radio astronomy techniques*, *Cosmic Research* **55** (2017) 1.

[7] H.A.S. Reid, *A review of recent type III imaging spectroscopy*, *Frontiers in Astronomy and Space Sciences* **7** (2020) 56.

[8] I.N. Sharykin, P. Kontar, E. and A. Kuznetsov, A., *LOFAR Observations of Fine Spectral Structure Dynamics in Type IIIb Radio Bursts*, *Sol. Phys.* **293** (2018) 115.

[9] N.N. Rahman, H. Cairns, I. and I. McCauley, P., *Spectropolarimetric Imaging of Metric Type III Solar Radio Bursts*, *Sol. Phys.* **295** (2020) 51.

[10] E.P. Carley, N. Vilmer and A. Vourlidas, *Radio Observations of Coronal Mass Ejection Initiation and Development in the Low Solar Corona*, *Frontiers in Astronomy and Space Sciences* **30** (2020) 51.

[11] A.T. Altyntsev, S.V. Lesovoi, M.V. Globa, A.V. Gubin, A.A. Kochanov, V.V. Grechnev et al., *Multiwave Siberian Radioheliograph*, *Solar-Terrestrial Physics* **6** (2020) 30.

[12] H. Nakajima, M. Nishio, S. Enome, K. Shibasaki, T. Takano, Y. Hanaoka et al., *The Nobeyama radioheliograph*, *Proc. IEEE* **82** (1994) 705.

[13] S.V. Lesovoi, A.T. Altyntsev, E.F. Ivanov and A.V. Gubin, *The multifrequency siberian radioheliograph*, *Sol. Phys.* **280** (2012) 651.

[14] S.V. Lesovoi, A.T. Altyntsev, E.F. Ivanov and A.V. Gubin, *A 96-antenna radioheliograph*, *Research in Astronomy and Astrophysics* **14** (2014) 864.

[15] L.V. Yasnov, V.M. Bogod and A.G. Stupishin, *Effective Gyroresonance Layers in the Transition Region of the Active Region of the Solar Atmosphere. Magnetic Fields and Heights*, *Astrophysical Bulletin* **75** (2020) 50.

[16] S.M. White, *Coronal Magnetic Field Measurements Through Gyroresonance Emission*, in *Solar and Space Weather Radiophysics. Astrophysics and Space Science Library*, D.E. Gary and C.U. Keller, eds., vol. 314, p. 89, 2004.